

Implicit Neural Representation for Mesh-Free Inverse Obstacle Scattering

Tin Vlašić^{*†}, Hieu Nguyen[†], Ivan Dokmanić[†]

^{*} Faculty of Electrical Engineering and Computing, University of Zagreb, Zagreb, Croatia

[†] Department of Mathematics and Computer Science, University of Basel, Basel, Switzerland

Email: tin.vlasic@fer.hr, {hieuhuu.nguyen, ivan.dokmanic}@unibas.ch

Abstract—Implicit representation of shapes as level sets of multilayer perceptrons has recently flourished in different shape analysis, compression, and reconstruction tasks. In this paper, we introduce an implicit neural representation-based framework for solving the inverse obstacle scattering problem in a mesh-free fashion. We efficiently express the obstacle shape as the zero-level set of a signed distance function which is implicitly determined by a small number of network parameters. To solve the direct scattering problem, we implement the implicit boundary integral method. It uses projections of the grid points in the tubular neighborhood onto the boundary to compute the PDE solution instead of a grid-size-dependent extraction method of surface points such as Marching Cubes. The implicit representation conveniently handles the shape perturbation in the optimization process. To update the shape, we use PyTorch’s automatic differentiation to backpropagate the loss function w.r.t. the network parameters, allowing us to avoid complex and error-prone manual derivation of the shape derivative. The proposed framework makes the inverse scattering problem more tractable with fewer parameters to optimize in comparison to the memory-inefficient grid-based approaches and outputs high-quality reconstruction results.

Index Terms—Helmholtz equation, implicit boundary integral method, inverse scattering problem, signed distance function

I. INTRODUCTION

In the inverse scattering problem [1]–[4], the scattering object is an obstacle with given boundary conditions and data, and the goal is to determine the obstacle from a set of measurements of the scattered field u^s . In this paper, we consider the sound-hard acoustic scattering problem (see Fig. 1) whose forward model is given by the Helmholtz equation:

$$\begin{aligned} (\Delta + k^2)u &= 0 \text{ in } \mathbb{R}^d \setminus \bar{\Omega}, \\ \frac{\partial u}{\partial n} &= 0 \text{ on } \partial\Omega, \end{aligned} \quad (1)$$

where Δ is the Laplacian operator, k is the wave number, Ω is the obstacle domain with boundary $\partial\Omega$, n is the outward unit normal to the boundary, and $u = u^i + u^s$ for u^i is an incident wave field. A method to solve the direct obstacle scattering problem is the integral equation method [2], [5]–[7]. By formulating the problem in terms of boundary integral equations, the method reduces the dimensionality of the problem and avoids the application of absorbing boundary conditions [2].

TV acknowledges support from the Swiss Government through the Swiss Federal Commission for Scholarships for Foreign Students (FCS), and the Croatian Science Foundation under Project IP-2019-04-6703. HN and ID were supported by the European Research Council Starting Grant 852821–SWING.

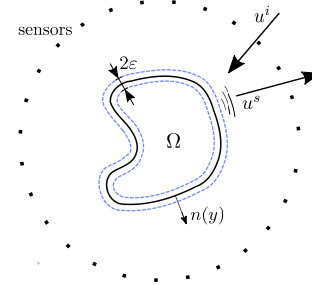


Fig. 1. Inverse scattering setup. u^i is the incident wave, u^s is the wave scattered by the obstacle (solid line). The sensors record the scattered waves at locations surrounding the obstacle. $n(y)$ is the normal vector at the point y . Dashed blue lines denote a thin tubular neighborhood around the boundary.

To solve the inverse scattering problem, we are interested in those methods that easily handle topological changes of the boundary. One such method is the implicit boundary integral method (IBIM) [8]–[10] which approximates the boundary integral via volume integral whose domain is implicitly represented by the signed distance function (SDF). Such a representation is advantageous in that it handles complicated shapes and their moving boundaries easily without the need for costly frequent remeshing, making the inverse problem more tractable [11]–[13]. Additionally, no a priori assumptions on the topology or the nature of the shape need to be made, e.g., the shape could be made of several disconnected subregions.

However, the grid-based representation of an SDF, especially in 3D space, is memory-inefficient. Recently, *implicit neural representations* of shapes [14]–[18], where a multilayer perceptron (MLP) $\eta_\theta : \mathbb{R}^d \rightarrow \mathbb{R}$ approximates the SDF, have shown remarkable results in data compression. Instead of being related to the fixed discretization of the ambient 3D space, the parameters θ of the MLP are directly related to the shape, whose watertight surface is implicitly represented by the isosurface of $\eta_\theta(x) = 0$. Among others, SIREN [19], which is an MLP architecture with periodic activation functions, fits SDFs of complicated shapes robustly.

In this paper, we propose using an implicit neural representation of an obstacle shape in the inverse scattering problem. It allows us to represent various shapes with the number of parameters smaller than the number of grid points of interest. Contrary to the deep learning shape optimization frameworks, such as [20], [21], where the Marching Cubes algorithm [22], [23] extracts the surface from the neural SDF on some prede-

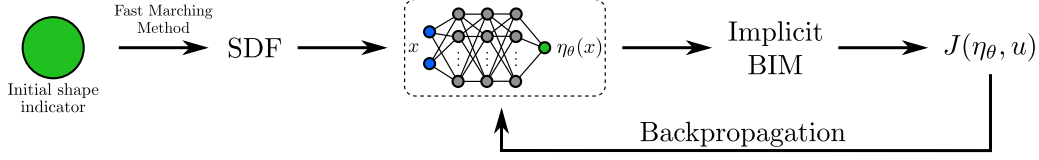


Fig. 2. **Shape reconstruction pipeline.** The MLP is first trained to represent an initial shape before being employed in the inverse problem. By using the neural SDF, we solve the direct problem to obtain the predicted scattered field. Minimization of the loss function updates network parameters, i.e., the shape.

finer grid prior to solving the PDE, we use the closest point formulation proposed in [8] and [9] for computing boundary integrals directly in the level set framework. The loss functional is composed of a data-fidelity term and penalty terms on the SDF to regularize the ill-posedness of the inverse obstacle scattering problem. We implement the proposed framework in PyTorch, making it differentiable throughout via automatic differentiation (AD). This allows for convenient gradient-based optimization of the parameters θ . While level-set methods are not new in the inverse scattering problems [24]–[26], to the best of our knowledge, implicit neural representations of shapes were not yet taken advantage of in such problems. Besides decreasing the number of parameters to optimize, a continuous parameterization with a SIREN offers additional benefits over grid-based representations such as analytical computation of gradients and higher-order derivatives that are independent of conventional grid resolutions. Finally, our differentiable programming framework is user friendly in that it avoids manual derivation of shape derivatives, it easily handles complicated shapes and their perturbations, and achieves good reconstruction results even in noise-corrupted setups.

II. DIRECT AND INVERSE OBSTACLE SCATTERING

The solution of (1) can be represented by the single layer potential [7]

$$u^s(x) = \mathcal{S}[\alpha](x) = \int_{\partial\Omega} \alpha(y) \Phi(x, y) ds(y) \text{ in } \mathbb{R}^d \setminus \partial\Omega, \quad (2)$$

where α is the density to match the boundary condition and Φ is the Green’s function for the Helmholtz equation. The density $\alpha \in C(\partial\Omega)$ satisfies a boundary integral equation

$$\int_{\partial\Omega} \alpha(y) \frac{\partial\Phi(x, y)}{\partial n(x)} ds(y) - \frac{1}{2}\alpha(x) = -\frac{\partial u^i}{\partial n}(x) \text{ on } \partial\Omega. \quad (3)$$

Finding a solution involves two steps: *i*) solving the linear system in (3) for $\alpha(x)$ and *ii*) evaluating (2). A key challenge is to accurately evaluate the boundary integral in (3) where $\partial\Omega$ is represented implicitly as the zero-level set of the SDF. This problem has been addressed in [8] and [9] where an effective solution involves a volume integration over the tubular neighborhood $T_\varepsilon = \{x \in \mathbb{R}^d : |\eta_\theta(x)| \leq \varepsilon \text{ and } \varepsilon > 0\}$, and a projection of the grid points in T_ε onto the boundary:

$$P_{\partial\Omega}(x) = x - \eta_\theta(x) \nabla \eta_\theta(x), \quad x \in T_\varepsilon, \quad (4)$$

since $|\nabla \eta_\theta(x)| = 1$ for all $x \in T_\varepsilon$ if $\partial\Omega$ is sufficiently smooth, and $n(x) = -\nabla \eta_\theta(x)$ for $\{x \in \mathbb{R}^d : \eta_\theta(x) = 0\}$. That way we avoid the need of extracting the surface by using grid-based techniques and/or the process of frequent remeshing.

The inverse obstacle scattering pipeline is depicted in Fig 2. Given M measurements $\hat{u}(x_m)$ for $x_m \in \mathbb{R}^d \setminus \Omega$, we minimize

$$J(\eta_\theta, u) = \frac{1}{M} \sum_{m=1}^M |u(x_m) - \hat{u}(x_m)|^2 + \mathcal{R}(\eta_\theta), \quad (5)$$

where the regularizer is

$$\mathcal{R}(\eta_\theta) = \lambda_1 \sum_{n=1}^N \left| |\nabla \eta_\theta(x_n)| - 1 \right|^2 + \lambda_2 \sum_{n=1}^N |\Delta \eta_\theta(x_n)|^2, \quad (6)$$

for $\{x_n\}$ are points in a region of interest (ROI). The ROI is selected to cover the obstacle and sampled so that we regularize the shape representation. The first term in (6) ensures that η_θ is an SDF and the second term imposes smoothness on the shape.

III. NUMERICAL EXPERIMENTS

We present results of numerical simulations for inverse obstacle scattering in 2D. The ROI was set as a square $[-1.1, 1.1]^2$ and sampled uniformly at 256×256 locations. We initialized the SIREN with 2 hidden layers and 128 hidden features, making it 33.5k parameters in total, and we trained the network using PyTorch [27] and Adam [28]. We measured the scattered field at M angular locations generated by scattering of multiple incident plane waves $u_i^i(x) = e^{jkx \cdot d_i}$ and multiple wave numbers k . We added a white Gaussian noise to some of the measurements and express the quality of the measurement data in terms of the signal-to-noise ratio (SNR). We show some of the reconstruction results for objects from [29] in Fig. 3 and 4. Reconstruction quality was assessed in terms of Chamfer distance between the ground truth point set S_{GT} and the reconstruction point set $S_{R,k}$ for different k s as:

$$d_{C,k}(S_{GT}, S_{R,k}) = \frac{1}{2} \left(\sum_{x \in S_{GT}} \min_{y \in S_{R,k}} \|x - y\|^2 + \sum_{y \in S_{R,k}} \min_{x \in S_{GT}} \|y - x\|^2 \right). \quad (7)$$

The results demonstrate the ability of the framework to achieve high-quality reconstructions and its robustness in the noise-corrupted and limited field-of-view (FOV) setups.

REFERENCES

- [1] A. Kirsch, *An Introduction to the Mathematical Theory of Inverse Problems*, 2nd ed. New York, NY: Springer, 2011.
- [2] D. L. Colton and R. Kress, *Integral Equation Methods in Scattering Theory*. Philadelphia: SIAM Publications, 2013.

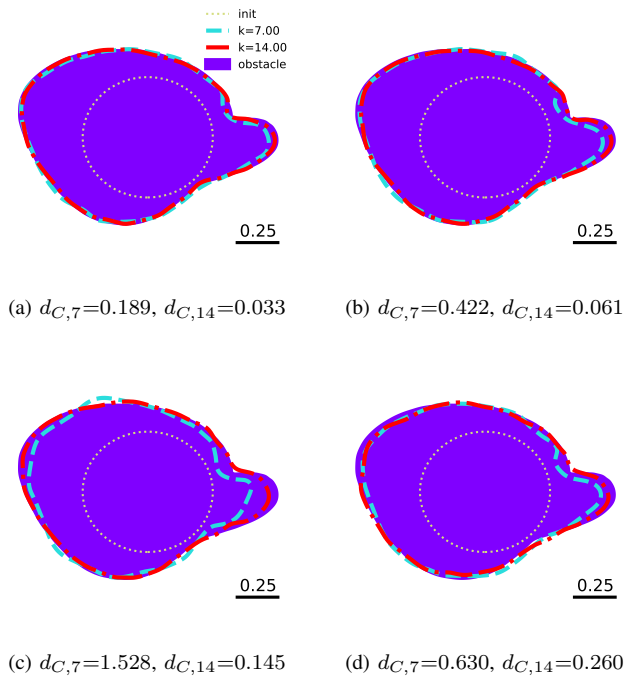


Fig. 3. **Reconstruction of a 2D cup obstacle.** (a) Full FOV noiseless measurements; (b) Full FOV noisy measurements (SNR = 20 dB); (c) Limited FOV noiseless; (d) Limited FOV noisy measurements (SNR = 25 dB). 96 sensors were uniformly displaced on a circle of radius 4.5 and the number of incident plane waves was 5. In limited FOV setups, sensors were uniformly placed in angular locations for intervals $[30^\circ, 150^\circ]$ and $[210^\circ, 330^\circ]$.

[3] —, “Looking back on inverse scattering theory,” *SIAM Review*, vol. 60, no. 4, pp. 779–807, 2018.

[4] —, *Inverse acoustic and electromagnetic scattering theory*, 4th ed. Cham: Springer, 2019.

[5] R. Kress, “Boundary integral equations in time-harmonic acoustic scattering,” *Mathematical and Computer Modelling*, vol. 15, no. 3-5, pp. 229–243, 1991.

[6] J. T. Katsikadelis, *Boundary elements: Theory and applications*. Amsterdam: Elsevier, 2002.

[7] G. B. Folland, *Introduction to partial differential equations*, 2nd ed. Princeton University Press, 2020, vol. 17.

[8] C. Kublik, N. M. Tanushev, and R. Tsai, “An implicit interface boundary integral method for Poisson’s equation on arbitrary domains,” *Journal of Computational Physics*, vol. 247, pp. 279–311, 2013.

[9] C. Chen and R. Tsai, “Implicit boundary integral methods for the Helmholtz equation in exterior domains,” *Research in the Mathematical Sciences*, vol. 4, no. 1, pp. 1–17, 2017.

[10] F. Izzo, O. Runborg, and R. Tsai, “Corrected trapezoidal rules for singular implicit boundary integrals,” *Journal of Computational Physics*, vol. 461, p. 111193, 2022.

[11] F. Santosa, “A level-set approach for inverse problems involving obstacles,” *ESAIM: Control, Optimisation and Calculus of Variations*, vol. 1, p. 17–33, 1996.

[12] S. Osher and R. Fedkiw, *Level Set Methods and Dynamic Implicit Surfaces*. Springer New York, 2003.

[13] M. Burger and S. J. Osher, “A survey on level set methods for inverse problems and optimal design,” *European Journal of Applied Mathematics*, vol. 16, no. 2, pp. 263–301, Jun. 2005.

[14] J. J. Park, P. Florence, J. Straub, R. Newcombe, and S. Lovegrove, “DeepSDF: Learning continuous signed distance functions for shape representation,” in *Proc. CVPR*, Jun. 2019.

[15] Z. Chen and H. Zhang, “Learning implicit fields for generative shape modeling,” in *Proc. CVPR*, Jun. 2019, pp. 5939–5948.

[16] L. Mescheder, M. Oechsle, M. Niemeyer, S. Nowozin, and A. Geiger, “Occupancy networks: Learning 3d reconstruction in function space,” in *Proc. CVPR*, 2019.

[17] M. Atzmon, N. Haim, L. Yariv, O. Israelov, H. Maron, and Y. Lipman, “Controlling neural level sets,” in *Proc. NeurIPS*, 2019, pp. 2032–2041.

[18] A. Gropp, L. Yariv, N. Haim, M. Atzmon, and Y. Lipman, “Implicit geometric regularization for learning shapes,” in *Proc. MLSys*, 2020, pp. 3569–3579.

[19] V. Sitzmann, J. N. Martel, A. W. Bergman, D. B. Lindell, and G. Wetzstein, “Implicit neural representations with periodic activation functions,” in *Proc. NeurIPS*, 2020.

[20] E. Remelli *et al.*, “MeshSDF: Differentiable iso-surface extraction,” in *Proc. NeurIPS*, vol. 33, 2020, pp. 22 468–22 478.

[21] B. Guillard *et al.*, “DeepMesh: Differentiable iso-surface extraction,” 2021, arXiv:2106.11795.

[22] W. E. Lorensen and H. E. Cline, “Marching cubes: A high resolution 3D surface construction algorithm,” *ACM SIGGRAPH Computer Graphics*, vol. 21, no. 4, pp. 163–169, Aug. 1987.

[23] J. A. Sethian, “Fast marching methods,” *SIAM Review*, vol. 41, no. 2, pp. 199–235, Jan. 1999.

[24] O. Dorn and D. Lesselier, “Level set methods for inverse scattering,” *Inverse Problems*, vol. 22, no. 4, pp. R67–R131, Jun. 2006.

[25] Z. Guo and M. V. de Hoop, “Shape optimization and level set method in full waveform inversion with 3D body reconstruction,” in *SEG Technical Program Expanded Abstracts 2013*, Aug. 2013.

[26] Y. F. Albuquerque, A. Laurain, and I. Yousept, “Level set-based shape optimization approach for sharp-interface reconstructions in time-domain full waveform inversion,” *SIAM Journal on Applied Mathematics*, vol. 81, no. 3, pp. 939–964, 2021.

[27] A. Paszke *et al.*, “Pytorch: An imperative style, high-performance deep learning library,” in *Proc. NeurIPS*, 2019, pp. 8024–8035.

[28] D. P. Kingma and J. Ba, “Adam: A method for stochastic optimization,” in *Proc. ICLR (Poster)*, 2015.

[29] B. Leibe and B. Schiele, “Analyzing appearance and contour based methods for object categorization,” in *Proc. CVPR*, 2003, pp. 402–409.

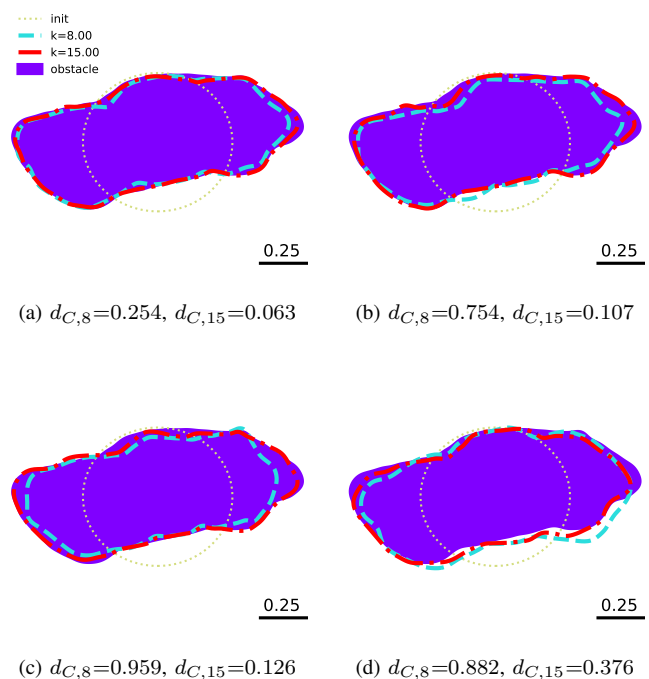


Fig. 4. **Reconstruction of a 2D car obstacle.** (a) Full FOV noiseless measurements; (b) Full FOV noisy measurements (SNR = 25 dB); (c) Limited FOV noiseless; (d) Limited FOV noisy measurements (SNR = 30 dB). 96 sensors were uniformly displaced on a circle of radius 4.5 and the number of incident plane waves was 5. In limited FOV setups, sensors were uniformly displaced in angular locations for intervals $[-60^\circ, 60^\circ]$ and $[120^\circ, 240^\circ]$.